Environ. Sci. Technol. **1998**, *32,* 3142−3148

Oxidative Degradation of 2,4,6-Trinitrotoluene by Ozone in an Electrohydraulic Discharge Reactor

P. S. LANG, W-K. CHING, D. M. WILLBERG, AND M. R. HOFFMANN*
W. M. Keck Laboratories, California Institute of Technology, Pasadena, California 91125

The electrohydraulic discharge process in the presence of ozone has been used to investigate the rapid degradation and mineralization of aqueous 2,4,6-trinitrotoluene (TNT) solutions that were directly exposed to high-energy electrical discharges between two submerged electrodes. The 165 μM solutions of TNT were completely (>90%) mineralized over the course of 300 electrical discharges of 7 kJ each. The kinetics of TNT degradation were investigated as a function of the aqueous-phase ozone concentration, pH, discharge energy, and electrode gap length. The rate of TNT degradation increases with an increase in aqueous-phase ozone concentration of up to 150 μM, an increase in pH from 3.0 to 7.9, an increase in discharge energy from 5.5 to 9 kJ, and a decrease in the electrode gap length from 10 to 6 mm. The rapid rates of mineralization (e.g. 12 ms) are attributed to the action of UV light in the reactor chamber on O_3 to produce a high flux of hydroxyl radicals per discharge (1 μM discharge^{-1}). The primary reaction intermediates were 2,4,6-trinitrobenzaldehyde and trinitrobenzene.

Introduction

Over the last decade, interest in the development of advanced oxidation technologies (AOTs) for the treatment of hazardous chemical wastes has grown enormously. Several AOTs involve the introduction of energy into aqueous solution via nonthermal processes. TiO_2 photocatlysis (*1*), electron-beam irradiation (*2, 3*), sonochemistry (*4*−*7*), and $UV/O_3/H_2O_2$ photolysis (*8*) are examples of this strategy. The electrohydraulic discharge process (EHD) is a nonthermal treatment technology that injects energy into an aqueous solution through a plasma channel formed by a high-current/high-voltage electrical discharge between two submerged electrodes (*9*−*15*). Industrial applications of the basic technology have included the simulation of underwater explosions (*15*), metal forming (*16*), rock fragmentation (*17*), and lithotripsy (*18*). In our previous paper (*19*), we examined the physical and chemical mechanisms in the pulsed-plasma discharge or electrohydraulic discharge process and evaluated the process as a unique alternative method for the treatment of hazardous wastes.

The electrohydraulic discharge events alone do not result in effective mineralization of aqueous-phase wastes (*19*). Most of the chemical effects of the pulsed discharges are due to direct and indirect photolysis and pyrolytic destruction in a high-temperature plasma channel (*19*). The photolytic effects result from the intense blackbody radiation given off by the hot plasma channel with an average temperature of $T_{avg} \approx$ 13 000 K during an underwater electrohydraulic discharge.

* Corresponding author phone: (626)395-4391; fax: (626)395-3170; e-mail: mrh@cco.caltech.edu.

In order to explore the effects of pulsed electrical discharges in the presence of O_3, we chose to examine the kinetics of degradiation of 2,4,6-trinitrotoluene (TNT). TNT is a priority EPA pollutant that is found in ambient environments primarily in the form of pink and red water at former munitions factory sites in the United States and in Europe (*20*−*25*). TNT has been shown to be a refractory compound, which is resistant to direct reaction with molecular ozone (*19*).

The Caltech EHD reactor has two principal components, which include a power supply connected to a 135 μF capacitor bank with control electronics and a 4-L discharge chamber that contains the solution to be treated (*19*). The capacitor bank can be discharged to net energies ranging from 2 to 25 kJ and then discharged through fast (300 ns rise time) ignitron switches into the electrode gap in the discharge chamber. The electrode gap in the reaction chamber (see Figure 1) is typically 8 mm and can be varied from 0 to 32 mm in length with an adjustable electrode assembly. The lifetime of the plasma channel under typical experimental conditions ranges from 20 to 100 μs (*19*). The EHD reactor system is, in effect, a large LRC circuit in which the discharge events often exhibit current reversal, and as a consequence, they are categorized as underdamped discharges. The reaction chamber has been designed to withstand the high-pressure shockwaves and the large electrical voltages and currents without electrical arcing or mechanical failure.

In the EHD process, chemical degradation occurs within the plasma channel directly due to pyrolysis and free radical reactions. However, the small volume of the plasma channel (1−3 mL) limits the amount of solution that can be treated directly by high-temperature pyrolytic processes. On the other hand, experiments with exploding wires have shown that electrohydraulic discharges induce extreme electromagnetic and mechanical conditions in the bulk solutions outside of the plasma channel region (*9*, *11*, *15*, *26*).

The plasma channel formed during an electrohydraulic discharge can reach temperatures of 14 000−50 000 K and thus functions as a blackbody radiation source with a maximum emittance in the vacuum ultraviolet VUV region of the spectrum (λ = 75−185 nm (*11*). The VUV emitted from the hot plasma is absorbed by the water layer immediately surrounding the plasma channel (*27*), and the UV light (λ > 184 nm) penetrates into the bulk of the solution. During the formation of the plasma channel (1−2 μs), an intense 5−20 kbar shockwave is generated due to the rapidly expanding plasma channel (*9*). The resulting shockwave can induce pyrolytic and free radical reactions indirectly via electrohydraulic cavitation (*18*). As the plasma channel cools over 1−3 ms, thermal energy is transferred to the surrounding water, resulting in the formation of a steam bubble (*15*). Within the steam bubble, the temperatures and pressures are high enough for the formation of transient supercritical water (*26*).

The simultaneous occurrence of multiple processes makes the chemistry of the EHD process extremely complicated. In an attempt to differentiate between these processes, we group them into *localized* and *extended* effects. We define oxidative degradation that occurs within the plasma channel and within the immediate vicinity as localized. This includes pyrolysis within the high-temperature plasma, oxidation due to direct and indirect VUV photolysis, and supercritical water oxidation. Oxidative degradation resulting from shockwaves and UV radiation in the bulk aqueous solution is defined as extended.

S0013-936X(98)00052-2 CCC: $15.00 © 1998 American Chemical Society
Published on Web 08/29/1998

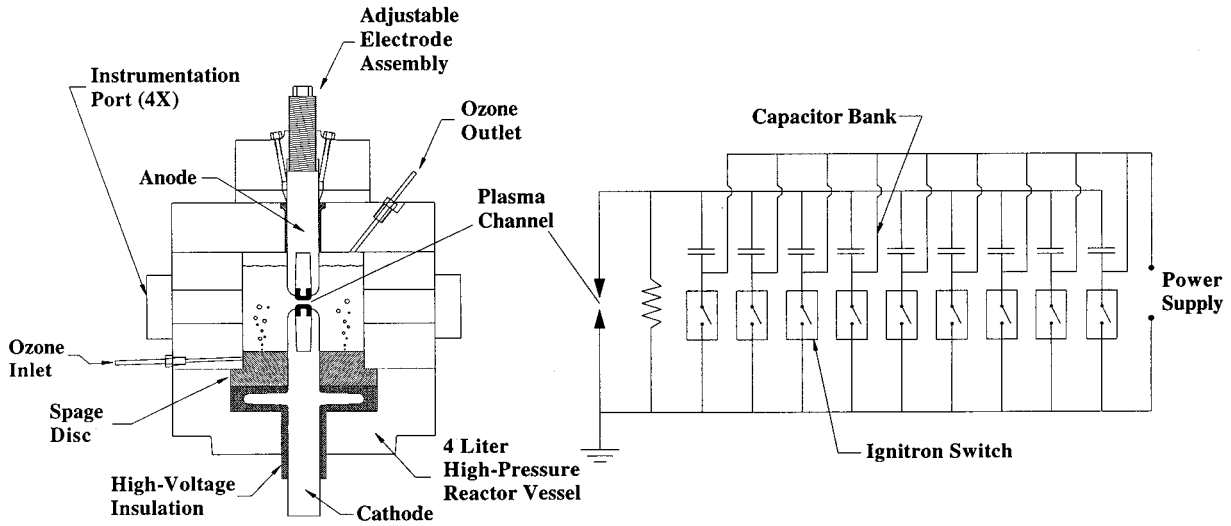

FIGURE 1. Schematic diagram of the EHD/O_3 reactor and electronic circuit.

Ozone is a powerful oxidant with a standard redox potential of 2.07 V, and it can react with organic and inorganic molecules in solution both directly and indirectly via its aqueous-phase degradation products such as the hydroperoxyl and hydroxyl radicals (*28*). When ozone is irradiated with ultraviolet light, it photolyzes to produce additional hydroxyl radicals via the reaction (*28*)

$$O_3 + h\nu \rightarrow O(^1D) + O_2 \quad (1)$$

$$O(^1D) + H_2O \rightarrow 2^{\bullet}OH \quad (2)$$

Thus, in the presence of water in either the gas or aqueous phase, ozone will photolyze to produce hydroxyl radicals, which are a stronger oxidizing agent with a standard redox potential of 2.7 V (*29*). Therefore, the combined ozone/UV process greatly enhances organic compound mineralization with respect to the ozone process alone. In our system, ozone was not observed to react directly with TNT over a 2-h time interval. However, TNT has been observed to react directly with the hydroxyl radical (*19*).

In our preliminary work with TNT, it was found that, in the absence of ozone, TNT was degraded via the electrohydraulic discharge technique by two effects: a zero-order direct photolysis combined with a first-order plasma channel effect. The overall rate of TNT degradation was thus described by eq 3 as follows (*19*):

$$\frac{dC}{dN} = -k_1 C_i - k_0 \quad (3)$$

where dC/dN is the change in concentration per discrete electrical discharge, C_i is the initial substrate concentration, k_0 is the zero-order term that accounts for direct photolysis, and k_1 is the first-order term that accounts for oxidation in the plasma channel region. For TNT in the absence of O_3, $k_0 = 0.10 \pm 0.03$ μM discharge^{-1} and $k_1 = (5.6 \pm 1.0) \times 10^{-4}$ discharge^{-1} (*19*).

The combined EHD/O_3 treatment of a 160 μM TNT solution was found to result in complete degradation of TNT and 34% reduction in TOC after 260 electrical discharges of 7 kJ each. The intrinsic rate constant of TNT degradation was observed to be 0.024 Ms^{-1} (*19*).

Experimental Methods

Pulsed-Power Plasma Reactor System. A schematic diagram of the essential features of the Caltech EHD reactor system is shown in Figure 1. The reactor chamber has been designed to withstand extreme electrical and mechanical stresses that are generated during an EHD event. Furthermore, it has been designed to provide reproducible conditions for >100 000 discharges. The high-voltage cathode bulkhead penetration assembly is the most critical component of the reactor. The insulation on the cathode has been designed to hold off a potential of at least 25 kV without shorting and to be resistant to the erosive effects of intense localized shockwaves.

An opposing electrode design was selected for shock resistance and adjustability. The adjustable ground electrode assembly allows for the precise control (±0.1 mm) of the spark gap length within a range of 0−30 mm; it maintains the structural integrity of the chamber; and it provides a tight compression connection for the high current pulses. The ground electrode can be readjusted to maintain a constant spark-gap separation to offset erosion of the electrode tips. Tantalum was selected for the electrode tips because it is a refractory metal (mp = 2996 °C) that minimizes electrode erosion; tantalum and its oxide are relatively inert and do not interfere significantly with the organic chemistry under investigation. The tantalum tips are joined to the steel electrodes by incorporating them into locking Morse taper assemblies. Flat cylindrical tips are used to minimize the effects of tip erosion during the lifetime of an experiment.

The electronics package that drives the pulsed discharge unit is an RLC circuit (Figure 1) designed and built by Pulsed-Power Technologies Inc. (PPTI, San Diego). It has been specifically designed with a low inductance (250−300 nH) and a relatively large capacitance (135 μF) to generate short but high-energy pulses. It is capable of delivering a 20-μs pulse with a total energy of 25 kJ and a peak power of up to 1 GW. Fast ignitron switches with a 300 ns risetime are used to trigger the discharge.

Electrical current was measured on the hot electrode bus (cathode) using a Rogowski coil that has been calibrated against a 123.3 $\mu\Omega$ current viewing resistor (T&M) Research). Voltages were measured on the cathode bus bar using a high-voltage probe (North Star Research). Triggering of the circuit and collection of the current and voltage traces was done remotely using a PC computer that was controlled with LabView software (National Instruments).

A single electrical discharge in the chamber can be described by the governing differential equation:

$$L\frac{d^2q}{dt^2} + R(t)\frac{dq}{dt} + \frac{q}{C} = 0 \quad (4)$$

where L is the inductance of the circuit, C is the capacitance, and q is the stored charge. R(t) is the resistance of the circuit and is dominated by the time-dependent resistance of the plasma channel. Depending on the specific values of R, L, and C, there are three regimes of discharge operation, underdamped $R < 2(L/C)^{1/2}$, critically damped $R = 2(L/C)^{1/2}$, and overdamped $R > 2(L/C)^{1/2}$. All discharges in our experiments were either underdamped or critically damped (i.e., most discharges exhibit current reversal).

In a typical EHD experiment, the large capacitor bank was charged to $V_{CB} = 10.2$ kV, which yielded the total stored energy of $E_{CB} = 7$ kJ. After complete charging, the capacitor bank was discharged very rapidly using the fast ignitron switches in order to charge the submerged electrodes. At a voltage of 10.2 kV, the electric field is insufficient to cause the formation of a plasma channel directly through liquid water. In this case, the resulting ionic current heats the water in the spark-gap, forming gas bubbles through which the discharge occurs (*13*). The pre-discharge current leakage significantly reduces the energy available for the discharge from an initial value of $E_{CB} = 7$ kJ to $E_D = 2$ kJ. After a plasma channel is formed, a current pulse arcs across the underwater spark-gap (0.8 cm). Since the plasma channel is the major resistive element in the circuit, the majority of the energy in the current pulse is deposited into the solution in the reactor chamber.

For experiments with 2,4,6-trinitrotoluene (TNT) in a reactor volume of 3.5 L, the total energy of the capacitor bank was set to $E_{CB} = 7$ kJ. The voltage on the cathode at the time of discharge was $V_D = 5.5 \pm 0.3$ kV; the energy delivered in the EHD pulse was $E_D = 2.0 \pm 0.2$ kJ. The peak current of these pulses was typically 90 kA. We used E_{CB} rather that E_D for all efficiency calculations, since it includes all of the energy losses due to the preliminary breakdown phenomenon. Furthermore, it is possible that thermal degradation of organic contaminants occurs during the preliminary breakdown phase.

We define the lifetime of an EHD pulse as the period of time between the first and last time the current pulse reaches 10% of its peak value. The duration of the pulse can be directly related to the voltage at the initiation of the plasma channel. In these experiments, the average current pulse lasted 41 ± 4 μs. Ozone is introduced into the chamber via 11 concentric 0.030 in. diameter holes in the HDPE ozone sparge liner at the base of the chamber.

Materials. $NaH_2PO_4 \cdot H_2O$ (EM Science) was used as received. TNT was obtained from the Naval Surface Warfare Center at Indian Head, MD, and recrystallized from 70 °C ethanol and washed in distilled ice water and dried before use. Ozone measurements were made using potassium 5,5,7-indigotrisulfonic acid (Sigma). All solutions were made with water obtained from a MilliQ-UV-Plus System ($R = 18.2$ $M\Omega$ cm^{-1}). Sodium nitrate was obtained from Baker and used as received.

$NaH_2PO_4 \cdot H_2O$ was added as an electrolyte to all the solutions to increase conductivity and to ensure a rapid formation of the plasma channel across the underwater electrode gap. An electrolyte concentration of 0.015 M was determined experimentally to be the minimum value to facilitate reproducible EHD discharges across a 0.8-cm spark-gap. NaH_2PO_4 was used because of its low reactivity with hydroxyl radicals ($k_{OH\cdot} = 2.0 \times 10^4$ M^{-1} s^{-1}) (*29*), which are produced during an electrohydraulic discharge.

Ozone was generated with an OREC Model V10-0 ozonator set at 3 AC amp with a flow rate of 1 L min^{-1}. The solution was sparged with ozone using a specially built HDPE insulating disk with 11 0.030 in, diameter vents. The ozone/O_2 mixture was pumped into the disk with a tube from the generator outside the chamber.

Analytical Procedures. The TNT concentration was determined using a Hewlett Packard Series II 1090 HPLC with a UV−VIS diode array detector and a reverse-phase column. Analysis was done within 4 h of the experiment. The reverse-phase column was a Hewlett-Packard Hypersil BDS column, and an isocratic 24:76 CH_3OH:H_2O mixture was used as the eluent at a flow rate of 0.725 mL/min; the analyzing wavelength for TNT was 226 nm. Samples were analyzed for total organic carbon (TOC) with a Shimadzu TOC-5000. Dissolved ozone concentrations were determined using the method of Bader and Hoigne (*30*). Samples were analyzed for nitrate by using a standard anion gradient elution program on a Dionex BioLC with a Dionex AS11 column.

Experimental Procedure. The kinetics of degradation of TNT were investigated parametrically as functions of [O_3], pH, discharge energy of the capacitor bank, and gap length between the electrodes. All degradation experiments were extended to 300 discharges (i.e., 12.3 ms total discharge time), so that complete degradation and mineralization of the TNT solution was achieved. The TNT concentration was not chosen as a parameter to investigate in this series of experiments because the effect of varying this parameter was already explored in a previous paper (*19*). Provided that a sufficiently large TNT concentration is used, the zero-order photolysis rate constant for TNT degradation will remain the same while the first-order plasma channel rate of decay will increase linearly with the TNT concentration. In all of the experiments, the solution chamber volume was 3.5 L so an open head space (0.5 L) was left in the chamber to facilitate mixing due to reflected shockwaves that produced a "depth-charge" effect.

The test solutions were sparged with ozone for 20 min prior to the onset of the discharge process so that a steady-state aqueous-phase ozone concentration could be achieved. During this pre-discharge ozone equilibration, time series samples were taken every 5 min to test for dark reactions of TNT with ozone. Samples were extracted with an 18-in. stainless steel needle and a clean plastic 10-mL syringe. The sample volumes were 10 mL for samples to be analyzed by TOC and HPLC and 5 mL for the indigo dye ozone samples. All samples were filtered through a 0.45-μm syringe filter before analysis. Total experimental run times were approximately 12 h, even though the net power utilization time was 12 ms.

The ozone concentration was varied by changing the current setting on the ozonator from 0 to 3 amp. The solution-phase ozone concentration was thus varied from 0 μM ozone to 165 μM. All other parameters were held constant during the experiments: pH = 4.7, $[TNT]_o = 170$ μM, and 300 EHDs at 7 kJ.

pH was varied by altering the background electrolyte concentration. A standard electrolyte solution of 15 mM for a conductance of 1.11 mS/cm was kept constant by adding either concentrated sodium hydroxide or concentrated phosphoric acid. The pH was varied from 2.95 to 7.91. In experiments where pH varied, it was necessary to keep the conductance constant since the conductance of the solution affects the electrohydraulic discharge characteristics and hence the energy partitioning of the circuit and the observed chemistry.

In experiments that were designed to explore the effect of discharge energy and electrode gap length on degradation of TNT, all parameters were held constant except the discharge energy of the capacitor bank and the electrode gap length: $[NaH_2PO_4] = 15$ mM, $[TNT]_o - 170$ μM, pH = 4.7, and conductance of 1.11 mS/cm, respectively. The discharge energy was varied from 5.5 to 9 kJ, and the electrode gap was varied from 6 to 10 mm.

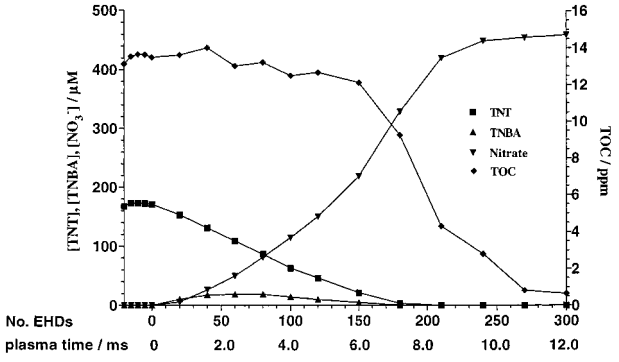

FIGURE 2. Full-scale degradation of a 3.5-L volume $[TNT]_o = 170$ μM (pH 4.7) in the presence of O_3 with 300 7-kJ electrohydraulic discharges (EHDs). The degradation intermediate, 2,4,6-trinitrobenzoic acid (TNBA), nitrate, and the total organic carbon (TOC) concentration also are shown.

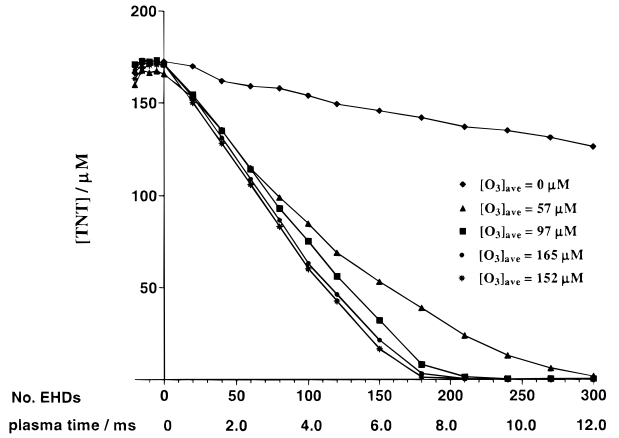

FIGURE 3. Degradation of 3.5 L of 170 μM TNT (pH 4.7) with 300 7-kJ electrohydraulic discharges (EHDs) as a function of aqueous phase $[O_3]$.

Results

Figure 2 shows the results of a full-scale degradation of TNT in the EHD reactor in which the electrode gap was 0.8 cm, $[NaH_2PO_4 \cdot H_2O] = 15$ mM, $E_{CB} = 7$ kJ, pH = 4.7, $K = 1.11$ mS/cm, and $Q(O_3) = 1.0$ L min^{-1}. TNT was completely degraded and mineralized to within experimental errors. The initial TNT concentration was 170 μM and was degraded totally over the range of 180−210 7 kJ electrohydraulic discharges. The solution TOC was initially 14 ppm and was reduced to less than 1 ppm over 270−300 electrohydraulic discharges. Nitrate concentrations were initially zero but rose with time to a value of 460 μM, which accounted for 90% of the initial TNT that was present in the solution. 2,4,6-Trinitrobenzoic acid was detected via HPLC as a degradation intermediate.

Additional experiments were performed under identical conditions to examine the effect of $[O_3]$. It is important to note that variations in both the gas- and aqueous-phase ozone content were changed during these experiments, although only the aqueous-phase ozone concentrations via the indigo dye technique are reported. The TNT degradation rates as a function of $[O_3]$ are shown in Figure 3.

In the absence of ozone but in the presence of O_2, the degradation of TNT was incomplete. By increasing the ozone content of the aqueous solution to an average value of 57 μM or higher, a complete degradation of TNT is achieved. Increasing $[O_3]$ above 150 μM had no further impact on the observed rates of TNT degradation.

Figure 4 shows the effect of varying the ozone concentration on the TOC degradation in the same set of experiments.

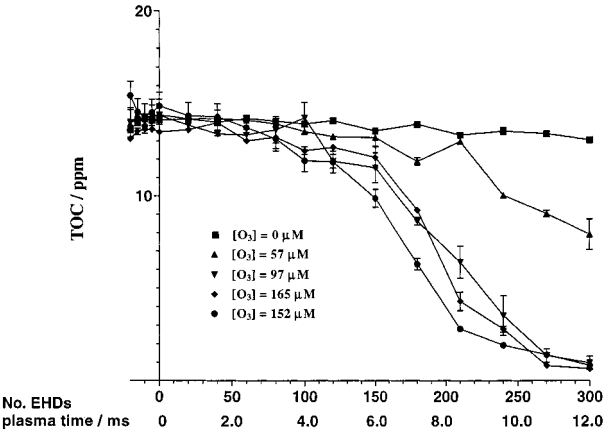

FIGURE 4. Total organic carbon (TOC) concentration profile in the presence of O_3 with 300 7-kJ electrohydraulic discharges (EHDs) as a function of $[O_3]$ for $[TNT]_o = 170$ μM at pH 4.7.

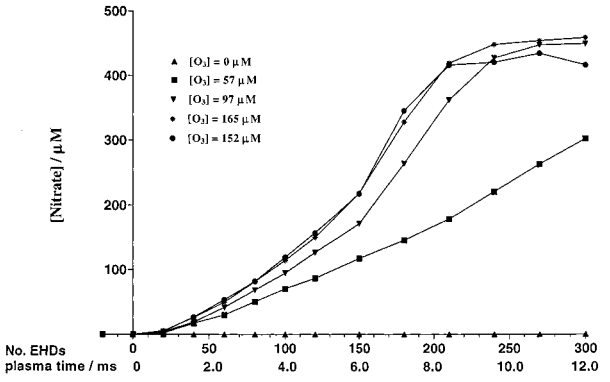

FIGURE 5. Nitrate production in the presence of O_3 with 300 7-kJ electrohydraulic discharges (EHDs) with variable O_3 concentrations for $[TNT]_o = 170$ μM and pH 4.7.

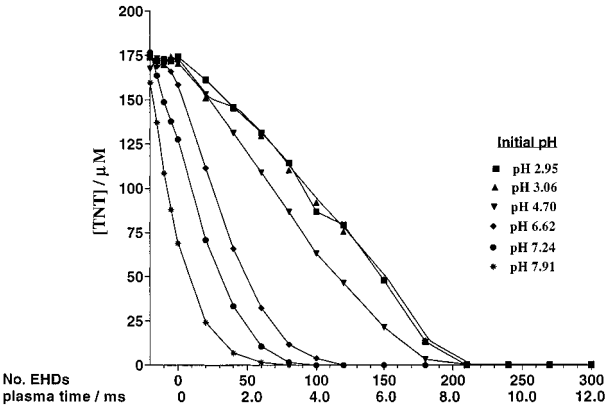

FIGURE 6. Degradation of 170 μM TNT solutions in the presence of O_3 with 300 7-kJ electrohydraulic discharges (EHDs) as a function of pH_o.

The effective extent of mineralization (i.e., conversion to NO_3^-, CO_2, and H_2O) is 90% with $[O_3] \geq 100$ μM. In the absence of O_3, no net mineralization was observed.

The effect of a variation in $[O_3]$ on the production of NO_3^- (Figure 5) was less than stoichiometric; however, when $[O_3^-] \geq 100$ μM, ~90% of the nitrogen present initially as TNT in solution was measured as NO_3^- by the end of the discharge sequence. In the absence of O_3^-, no NO_3^- was produced.

The effects of pH on TNT degradation are shown in Figure 6. Below pH 3, the degradation rate appears to be insensitive to pH, while above pH 5.0 a 3-fold enhancement in the overall rate of degradation was observed.

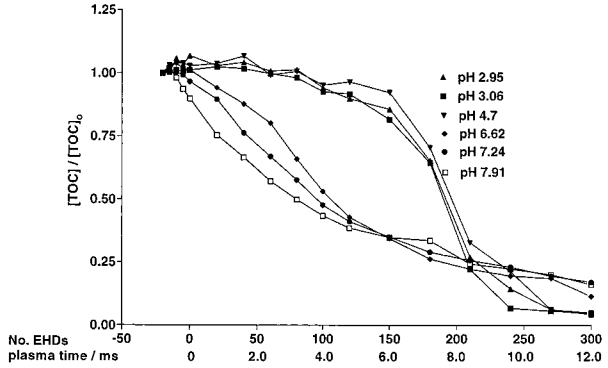

FIGURE 7. Total organic carbon (TOC) degradation in the presence of O_3 vs the number of 7-kJ electrohydraulic discharges as a function of solution pH.

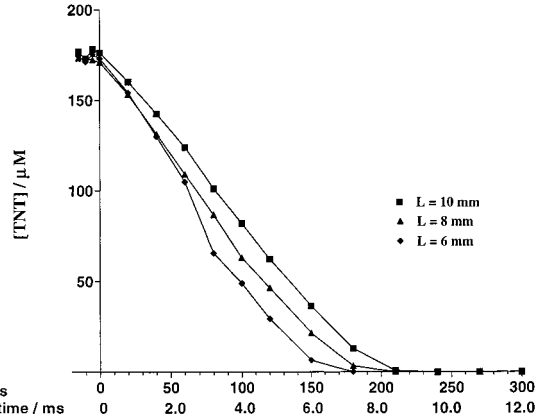

FIGURE 8. Degradation of 170 μM TNT solutions (pH 4.7) in the presence of O_3 with 300 7-kJ electrohydraulic discharges (EHDs) as a function of variable electrode gap length, *L*.

These results indicate that the reactions between TNT and the primary ozone decay product (•OH) becomes more important at high pH. In Figure 6, the data points seen before zero discharges are from the 20-min pre-sparge time that brings the solution-phase ozone concentration to a steady-state value. The O_3 degradation products (i.e., •OH) are thus responsible for the TNT degradation before the pulsed discharges are more so during the sequential discharges. It is clear that the reaction of •OH with TNT is responsible for the enhanced rate of TNT degradation at pH > 6.0.

The apparent lower degradation rate of TNT at pH 3 relative to pH 4.7 (Figure 6) may be independent of O_3 chemistry and may only be a function of pH effects on the electrohydraulic discharge process. A series of control experiments were performed at a constant solution conductance of 1.11 mS/cm, which is the conductance of all the solutions in the pH experiments, but at various pH values. These results suggested that at pH < 3.5 the water in the electrode gap may be more highly structured and, as a result, the process of a plasma channel formation may be less energetically favorable.

For a plasma channel to form, the water in the electrode gap must be vaporized by a pre-discharge ionic leakage current. A more highly structured water in the electrode gap will require more energy to initiate the discharge. Thus, at pH < 3.5, a larger portion of the energy is used to form the plasma channel while less energy is actually deposited into the chamber.

Similar results were seen in the TOC vs time profiles of Figure 7. For example, TNT mineralization at pH 6.6−7.9 is enhanced when compared to the rate at pH 4.7. Despite the increase in the mineralization rate observed for the pH 6.6−7.9 range, the final extent of mineralization of the test solutions was approximately the same.

A series of experiments were conducted to investigate the dependence of the TNT degradation rates on the electrode gap length in the reaction chamber (Figure 8). All parameters in these experiments were held constant at standard values cited above except that electrode gap length was varied over the range of 6−10 mm. As can be seen from the data of Figure 8, the length of the electrode gap over which the discharge takes place has a significant impact upon the rate of TNT conversion. The time for complete conversion of TNT at a 6-mm electrode gap is the shortest, while time of the conversion for the 10-mm gap is the longest. With a smaller electrode gap it is easier to form the plasma channel, and more energy can be deposited into solution, which leads indirectly to photochemical and plasma channel effects and subsequently to a faster overall degradation and mineralization of TNT. With a larger electrode gap, more energy is required for plasma channel formation, and less energy is actually deposited into the chamber for TNT degradation.

A series of experiments were performed to investigate the effect of the discharge energy upon the rate of conversion and mineralization of TNT Figure 9. These data show that the initial discharge energy has a significant impact on how rapidly solutions of TNT are degraded. If discharge energy are higher than 7 kJ, then a more rapid conversion of TNT occurs. If the discharge energy is lower, then a lower rate of TNT conversion occurs. At higher initial discharge energy, more energy is deposited into the electrode gap, and at lower initial discharge energy, less energy is deposited into the electrode gap. Thus, greater chemical effects are measured at higher discharge energies.

In the absence of O_3, degradation rates can be expressed in terms of eqs 5 and 6 (*19*):

$$C(N) = a^N C_i - k_0 \sum_{n=0}^{N-1} a^n \quad (5)$$

$$\frac{dC}{dN} = -k_1 C_i - k_0 \quad (6)$$

where C_i is the substrate concentration, k_1 is the first-order plasma channel degradation rate constant, k_0 is the zero-order photolysis rate constant, a is the volume fraction not treated per discharge by the plasma channel, and N is the number of electrohydraulic discharges. $k_1$and k_0 are determined from a series of kinetic runs. For TNT, the values of these zero-order and first-order rate constants under standard experimental conditions are $k_0 = 0.10 \pm 0.03\,\mu$M discharge^{-1} and $k_1 = (5.6 \pm 1.0) \times 10^{-4}$ discharge^{-1}.

Ozone has a very low reaction rate constant with TNT, and under standard conditions, ozone will not react appreciably with TNT over the net time of 2 h that is required to complete an electrohydraulic discharge experiment. Therefore, no additional terms are needed to reflect direct reaction between ozone and TNT.

However, an additional term needs to be added to eq 6 to reflect the contribution of the O_3 degradation reactions. This contribution can be described by a zero-order term representing the hydroxyl radical dose per electrohydraulic discharge in the reaction chamber. Ozone in both the aqueous and gas phases in the reaction chamber undergoes photolysis to produce hydroxyl radicals. During the discharge, the plasma channel acts as an intense blackbody radiator that gives off a powerful 20−100-μs burst of UV and VUV radiation (*19*). The UV radiation given off is absorbed by the aqueous-phase and gas-phase ozone in the chamber and produces a flux of •OH radicals. Following the burst of UV radiation from the plasma channel, a powerful shock

wave travels through the solution and its air−water interface to mix the gaseous and liquid contents of the reaction vessel.

The addition of ozone to the EHD chamber effectively acts as an added source of hydroxyl radicals. The data during these degradations can be quantified as follows:

$$C(N) = a^N C_i - k_0' \sum_{n=0}^{N-1} a^n \quad (7)$$

$$\frac{dC}{dN} = -k_1 C_i - k_0' \quad (8)$$

$$k_0' = k_0 + k_{OH} \quad (9)$$

where k_{OH} is the zero-order rate constant for the hydroxyl radical term in the reaction vessel. Note that the zero-order rate constant for the reaction of hydroxyl radicals is zero-order only when plotted against the number of electrohydraulic discharges. Between any two EHDs there is 10 s of time during which the power supply is recharging. Thus, even though the reaction of hydroxyl radicals with TNT is a fast apparent first-order chemical reaction (due to the mass-transfer limited production of •OH) in real time, it appears as zero order when plotted against the number of EHDs.

The average value for the zero-order hydroxyl radical rate constant can be obtained by the difference between eqs 8 and 6. The present data yields a value for k_{OH} of 1.0 μM discharge^{-1}.

2,4,6-Trinitrobenzoic acid was identified as the principal reaction intermediate (see Figure 2) during TNT degradation while trinitrobenzene was detected at trace levels. 2,4,6-Trinitrobenzaldehyde was not quantified due to the lack of an HPLC standard. A reaction mechanism that is consistent with our observed reaction intermediates and products may occur as follows:

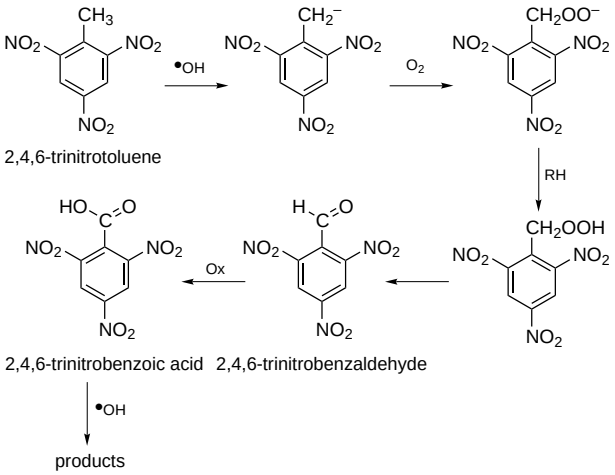

A similar mechanism was proposed by Schmelling and Gray (*31*) for the photocatalytic degradation of TNT. The final observed products were water, nitric acid, and carbon dioxide produced according to the following stoichiometry:

$$C_7H_5O_6N_3 + 9O_2 \rightarrow 3HNO_3 + 7CO_2 + H_2O \quad (10)$$

The kinetic data presented in this paper demonstrate that the EHD/O_3 process can completely degrade TNT and achieve the effective mineralization of TNT solutions (>90%). The final products of the degradation are nitric acid, carbon dioxide, and water. The intermediate degradation products formed subsequent to ring cleavage were not investigated in this current work but will be the subject of future investigations. They are likely short-chain carboxylic acids and amides, as not all of the nitrogen was accounted for by mass balance in the degradations.

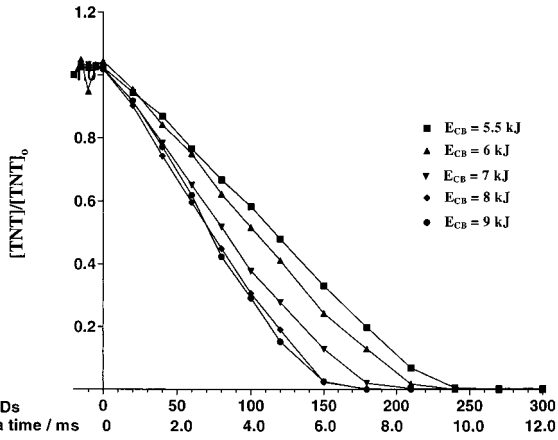

FIGURE 9. Degradation of TNT in the presence of O_3 with 300 electrohydraulic discharges (EHDs) as a function of discharge energy.

A number of the other processes have been used to degrade TNT: TiO_2 photocatalysis (*31*−*34*), bioremediation (*35*−*44*), UV photolysis (*45*), UV/ozone (*46*), and UV/O_3/H_2O_2 combinations (*47*). Biological treatment of TNT and direct UV photolysis both result in complex mixtures of reaction products with unknown identities and toxicities and do not lead to complete mineralization. TiO_2 photocatalytic treatment of TNT leads to the complete mineralization of TNT under aerobic conditions over periods of 1−2 h. Treatment of TNT with both UV/O_3 and UV/H_2O_2 processes can also lead to mineralization of TNT with treatment times on the order of 1−2 h. Thus, the UV/O_3, UV/H_2O_2, TiO_2 photocatalytic, and EHD/O_3 processes are all capable of TNT mineralizations at the laboratory test level over periods of approximately 2 h.

An interesting aspect of the EHD/O_3 process that has not yet been explored is the potential for the rapid treatment of aqueous-phase wastes. In this present work, a 3.5-L solution of 160 μM TNT was treated with 300 discharges at E_{CB} = 7 kJ in a period of 2 h. The present repetition rate of the charging circuit is 0.1 Hz. The total plasma utilization time assuming 300 EHDs at 40 μs/EHD is 12 ms. With currently existing technology, a discharge circuit could be built that can deliver 7-kJ discharges at 10 Hz, and a 2-Hz machine is available for our use at the present time. Thus, the total treatment time for a 3.5-L solution of 160 μM TNT could easily be reduced from 2 h to 0.5−2.5 min. The ozone utilization efficiency in this system would also be increased by a factor of 100 as most of the ozone introduced into the current system is not used to produce hydroxyl radicals.

The observed energy efficiency for TNT mineralization in the EHD/O_3 system, accounting for both the energy costs of the electrohydraulic discharge apparatus and the ozonator, is 1.4×10^{-14} J/molecule or 8.7×10^6 kJ/mol. Assuming a current power consumption cost of 11¢/KWH and a solution concentration of 160 μM, the cost of mineralizing TNT in our system is $266/mol of TNT or 4.3¢/L.

To improve the energy efficiency of the EHD/O_3 process, it is crucial to determine the origin of the hydroxyl radicals in the EHD chamber that are producing the observed TNT degradation and mineralization. The observed flux of hydroxyl radicals per electrohydraulic discharge has two sources: photolysis of aqueous-phase ozone and photolysis of gas-phase ozone. It must be determined via future experiments what fraction of the net hydroxyl radical flux per EHD is originating from each source to maximize the efficiency of the system. If it turns out that the majority of

hydroxyl radicals are originating from photolysis of gas-phase ozone, then the reactor geometry must be reconfigured to maximize the photolysis of gas-phase vs aqueous-phase ozone. Future experiments will be conducted to determine how the observed hydroxyl radical flux per EHD is partitioned between photolysis of aqueous-phase vs gas-phase ozone.

Acknowledgments

Financial support from the Advanced Research Projects Agency (Grant NAV5HFMN N0001492J1901), the Office of Naval Research, and the Electric Power Institute (Grant RP 8003-37) is gratefully acknowledged.

Literature Cited

(1) Hoffmann, M. R.; Martin, S. T.; Choi, W. Y.; Bahnemann, D. W. *Chem. Rev.* **1995**, *95*, 69.
(2) *Non-Thermal Plasma Techniques for Pollution Control Part A: Overview, Fundamentals and Supporting Technology*; Penetrante, B. M., Schultheis, S. E., Eds.; Springer-Verlag: New York, 1993.
(3) *Non-Thermal Plasma Techniques for Pollution Control Part B: Electron Beam and Electrical Discharge Processing*; Penetrante, B. M., Schultheis, S. E., Eds.; Springer-Verlag: New York, 1993.
(4) Kotronarou, A.; Mills, G.; Hoffmann, M. R. *J. Phys. Chem.* **1991**, *95*, 3630.
(5) Hua, I.; Höchemer, R. H.; Hoffmann, M. R. *Environ. Sci. Technol.* **1995**, *29*, 2790.
(6) Hua, I.; Höchemer, R. H.; Hoffmann, M. R. *J. Phys. Chem.* **1995**, *99*, 2335.
(7) Serpone, N.; Terzian, R.; Hidaka, H.; Pelizzetti, E. *J. Phys. Chem.* **1994**, *98*, 2634.
(8) Legrini, O.; Oliveros, E.; Braun, A. M. *Chem. Rev.* **1993**, *93*, 671.
(9) Martin E. A. *J. Appl. Phys.***1958**, *31*, 255.
(10) Robinson, J. W. *J. Appl. Phys.***1967**, *38*, 210.
(11) Robinson, J. W.; Ham, M.; Balaster, A. N. *J. Appl. Phys.***1973**, *44*, 72.
(12) Robinson, J. W. *J. Appl. Phys.***1973**, *44*, 76.
(13) Naugolnykh, K. A.; Roy, N. A. *Electrical Discharges in Water. A. Hydrodynamic Description*; Technical Report FTD-HC-2049-74; Foreign Technology Division, Wright-Patterson Air Force Base: Dayton, OH, 1974.
(14) Radovanov, S. B. A Spectroscopic and Thermodynamic Study of Pulsed Underwater Discharges. In *The Physics of Ionized Gases*; Tanović, L., Konjević, N., Eds.; Nova Science Publishers: Commack, NY, 1988.
(15) Buntzen, R. R. The Use of Exploding Wires in the Study of Small-Scale Underwater Explosions. In *Exploding Wires*, Vol. 2; Chace, W. G., Moore, H. K., Eds.; Plenum Press: New York, 1962; p 195.
(16) Smith, K. F. Electro-Hydraulic Forming. In *High-Velocity Forming of Metals*; Wilson, F. W., Ed.; Prentice Hall: Englewood Cliffs, NJ, 1964; p 77.
(17) Wesley, R. H.; Ayres, R. A. U.S. Patent No. 4,479,680, **1984**.
(18) Coleman, A. J.; Saunders, J. E.; Crum, L. A.; Dyson, M. *Ultrasound Interact. Med. Biol.* **1987**, *13*, 69.
(19) Willberg, D. M.; Lang, P. S.; Höchemer, R. H.; Kratel, A.; Hoffmann, M. R. *Environ. Sci. Technol.***1996**, *30*, 2526.
(20) Chen, T. H.; Campbell, C.; Fisco, W. J. Characterization of Pollutants at Holston Army Ammunition Plant. U.S. Army ARRADCOM, 1981.
(21) Conley, K. A.; Mikucki, W. J. Migration of Explosives and Chlorinated Pesticides in a Simulated Sanitary Landfill. Construction Engineering Research Laboratory, 1976.
(22) Hall, T. N.; Lawrence, G. W. A Study of the Organic Components of Red Water: Naval Surface Weapons Center, 1976.
(23) Kobylinski, E. A.; Burrows, W. D. Tertiary Treatment of Effluent from Holston AAP Industrial Liquid Waste Treatment Facility II. Corona Oxidation Studies: TNT, RDX, HMX TAX, and SEX. U.S. Army Medical Bioengineering Research and Development Laboratory, 1983.
(24) Spanggord, R. J.; Gibson, B. W.; Keck, R. G.; Thomas, D. W.; Barkley, J. J. J. *Environ. Sci. Technol.* **1982**, *16*, 229.
(25) Spanggord, R. J.; Suta, B. E. *Environ. Sci. Technol.* **1982**, *16*, 233.
(26) Ben'kovskii, V. G.; Golubnichii, P. I.; Maslennikov, S. I. *Sov. Phys. Acoust.* **1974**, *20*, 14.
(27) Jakob, L.; Hashem, T. M.; Burki, S.; Guindy, N. M.; Braun, A. M. *J. Photochem. Photobiol. A: Chem.* **1993**, *7*, 97.
(28) Horvath, M.; Bilitzky, L.; Huttner, J. *Ozone*; Elsevier: New York, 1985; p 119.
(29) Buxton, G. V.; Greenstock, C. L.; Helman, W. P.; Ross, A. B. *J. Phys. Chem. Ref. Data* **1988**, *17*, 516.
(30) Bader, H.; Hoigne, J. *Water Res.* **1981**, *15*, 449.
(31) Schmelling, D. C.; Gray, K. A. *Water Res.* **1995**, *29*, 2651.
(32) Dillert, R.; Fornefett, I.; Siebers, U.; Bahnemann, D. *J. Photochem. Photobiol. A* **1996**, *94*, 231.
(33) Schmelling, D. C.; Gray, K. A.; Kamat, P. V. *Environ. Sci. Technol.* **1996**, *30*, 2547.
(34) Wang, Z.; Kutal, C. *Chemosphere* **1995**, *30*, 1125.
(35) Haïdour, A.; Ramos, J. L. *Environ. Sci. Technol.* **1996**, *30*, 2365.
(36) Boopathy, R.; Kulpa, C. F.; Wilson, M. *Appl. Microbiol. Biotechnol.* **1993**, *39*, 270.
(37) Bumpus, J. A.; Tatarko, M. *Curr. Microbiol.* **1994**, *28*, 185.
(38) Duque, E.; Haïdour, A.; Godoy, F.; Ramos, J. L. *J. Bacteriol.* **1993**, *175*, 2278.
(39) Spiker, J. K.; Crawford, D. L.; Crawford, R. L. *Appl. Environ. Microbiol.* **1992**, *58*, 3199.
(40) Boopathy, R.; Kulpa, C. F. *Curr. Microbiol.* **1992**, *25*, 235.
(41) Sublette, K. L.; Ganapathy, E. V.; Schwartz, S. *Appl. Biochem. Biotechnol.* **1992**, *34*, 709.
(42) Preuss, A.; Fimpel, J.; Diekert, G. *Arch. Microbiol.* **1993**, *159*, 345.
(43) Boopathy, R.; Manning, J.; Montemagno, C.; Kulpa, C. *Curr. Microbiol.* **1994**, *28*, 131.
(44) Boopathy, R. *Arch. Microbiol.* **1994**, *162*, 167.
(45) Burlinson, N. E.; Sitman, M. E.; Kaplan, L. A.; Kayser, E. *J. Org. Chem.* **1979**, *44*, 3695.
(46) Sierka, R. A. *Ozone: Sci. Eng.* **1985**, *6*, 275.
(47) Andrews, C. C. *Photooxidative Treatment of TNT Contaminated Waste Water*; Report WQEC/C 80-137; Weapons Quality Engineering Center, Naval Weapons Support Center: Crane, IN, 1980.

Received for review January 21, 1998. Revised manuscript received June 2, 1998. Accepted July 3, 1998.

ES980052C